Photoionization of potassiumlike transition-metal ions: Ti^{3+} to Fe^{7+}

A. M. Sossah, H.-L. Zhou, and S. T. Manson
Department of Physics and Astronomy, Georgia State University, Atlanta, Georgia 30303, USA
(Received 28 June 2010; published 18 October 2010)

Photoionization cross-section calculations are performed on potassiumlike transition metal ions (Ti^{3+}, V^{4+}, Cr^{5+}, Mn^{6+}, and Fe^{7+}) using both nonrelativistic (*LS*-coupling) and relativistic (Breit-Pauli) *R*-matrix methods for the ground ($[Ne]3s^2 3p^6 3d\ ^2D^e_{3/2}$) and the first excited ($[Ne]3s^2 3p^6 3d\ ^2D^e_{5/2}$) states of each of the five ions, along with the excited $4s\ ^2S$ state of Ti^{3+}. Photon energies up to the first $3p$ ionization threshold are considered. The results show that for Ti^{3+}, the cross sections are dominated by the giant ($3p \rightarrow 3d$) resonances which are analyzed and identified, while for the four other ions (V^{4+}, Cr^{5+}, Mn^{6+}, and Fe^{7+}), the $3p \rightarrow 3d$ resonances lie below the ionization threshold, and the cross sections are dominated by $3p^5 3dnd$ and $3p^5 3dn's$ Rydberg series of resonances. Comparison of the Ti^{3+} results with available theoretical and experimental data shows good agreement.

DOI: 10.1103/PhysRevA.82.043416 PACS number(s): 32.80.Fb, 32.80.Aa, 32.80.Zb

I. INTRODUCTION

Investigating dynamical processes involving atoms and ions with open $3d$ subshells has been a source of great interest and challenge for several years if not decades. $3d$ transition metal atoms and ions hold particular interest owing to the open $3d$ subshell which allows the possibility of giant dipole resonances [1] resulting from $3p \rightarrow 3d\ \Delta n = 0$ transitions, and an understanding of these dynamical processes can serve as a springboard for the understanding of the dynamical process of all open *d*-subshell and *f*-subshell atoms and ions in general. The challenge is the serious difficulty that both theorists and experimentalists have faced in connection with those transition metal atoms and ions; the principal cause of this challenge is the high sensitivity of the $3d$ orbital to its environment, making calculations on these atoms and ions extremely difficult. However, during the last few decades, the advent of third-generation synchrotron radiation sources [2], the development of new techniques and tools [3,4], and the extremely rapid development of computational power have produced significant advances in the investigation of dynamical atomic processes, and open *d*-subshell and *f*-subshell atoms and ions have been subject to increasing interest both theoretically and experimentally. Among the dynamical process of interest is the response of these atoms and ions to ionizing radiation, the photoionization process, which is of interest as a fundamental process of nature, along with applications to a number of areas of science and technology, most notably the modeling of plasmas, astrophysical, and otherwise.

In this work we report on the first part of a study of the photoionization of potassiumlike transition metal ions for nuclear charges Z from 22 to 26 (Ti^{3+}, V^{4+}, Cr^{5+}, Mn^{6+}, and Fe^{7+}); those ions belong to what is known as the iron group. The presence of Ti^{3+} ions with the other four ions (V^{4+}, Cr^{5+}, Mn^{6+}, and Fe^{7+}) is guided by our intention to show the profound difference that can occur in photoionization spectra of members of the same isoelectronic sequence, here the potassium isolectronic sequence.

The photoionization of an atomic system A (Ti^{3+}, V^{4+}, Cr^{5+}, Mn^{6+}, and Fe^{7+}) is given schematically as

$$A + h\nu \rightarrow A^+ + e, \tag{1}$$

which is the direct photoionization pathway. In addition, however, the photoionization can proceed through an intermediate resonance; this pathway is represented as

$$A + h\nu \rightarrow (A)^* \rightarrow A^+ + e. \tag{2}$$

While we are primarily interested in photoionization of those various atomic systems A (Ti^{3+}, V^{4+}, Cr^{5+}, Mn^{6+}, and Fe^{7+}) in their ground state in this work, the initial states of each ionic species A considered in the relativistic calculations are both the ground $[Ne]3s^2 3p^6 3d\ ^2D^e_{3/2}$ plus the first excited states $[Ne]3s^2 3p^6 3d\ ^2D^e_{5/2}$, and for Ti^{3+} ions, the excited state $[Ne]3s^2 3p^6 4s\ ^2S^e_{1/2}$ is also considered in our calculations. The states of the final state ion A^+ are known in *R*-matrix language as the target states, with $N = 18$ electrons; those target ions are combined with the free electron to form the total final state, an $(N + 1) = 19$ electron system. By dipole selection rules, the total final state (target state + unbound electron) can have (nonrelativistic symmetries) $^2P^o$, $^2D^o$, and $^2F^o$, that is, the nonrelativistic allowed transitions are given by

$$\begin{aligned} {}^2D^e &\rightarrow {}^2P^o, {}^2D^o, {}^2F^o, \\ {}^2S^e &\rightarrow {}^2P^o. \end{aligned} \tag{3}$$

In the relativistic case, transitions (3) become

$$\begin{aligned} {}^2D^e_{3/2} + h\nu &\rightarrow {}^2P^o_{1/2}, {}^2P^o_{3/2}, {}^2D^o_{3/2}, {}^2D^o_{5/2}, {}^2F^o_{5/2}, \\ {}^2D^e_{5/2} + h\nu &\rightarrow {}^2P^o_{3/2}, {}^2D^o_{3/2}, {}^2D^o_{5/2}, {}^2F^o_{5/2}, {}^2F^o_{7/2}, \\ {}^2S^e_{1/2} + h\nu &\rightarrow {}^2P^o_{1/2}, {}^2P^o_{3/2}. \end{aligned} \tag{4}$$

The target state (Ti^{4+}, V^{5+}, Cr^{6+}, Mn^{7+}, and Fe^{8+}) orbitals, in the present work, are obtained using the program AUTOSTRUCTURE [5–8]; the target state wave functions and their energy levels are determined from configuration-interaction (CI) calculation using these orbitals. The nonrelativistic (*LS*-coupling scheme) and the relativistic (Breit-Pauli) *R*-matrix methods [8,9] are employed to carry out the photoionization cross-section calculations. For the Ti^{3+} ion photoionization study, in addition to the calculations, the resonances in the region of the giant $3p \rightarrow 3d$ excitations are analyzed (position, width, and identification) using the QB code [10–12], and theoretical photoionization cross-section

and resonance analysis results are compared with available experimental and theoretical data [13,14] in the case of Ti^{3+}.

II. THEORY AND METHOD OF CALCULATION

As mentioned previously, the photoionization calculations were performed within the framework of the *R*-matrix methodology which was felt to be the most appropriate for this work for a variety of reasons. First, the existence of both relativistic and nonrelativistic versions allows us the opportunity to spotlight relativistic effects by performing the calculations both ways. Second, since the *R*-matrix method is a "partitioned-space" theory, it allows us to include a great deal of correlation in the wave functions in the inner region (where correlation is most important) and omit correlation in the outer region, thereby allowing the inclusion of the important aspects of correlation while keeping the calculation tractable. Third, the *R*-matrix theory is equally applicable to atomic and ionic systems of any structure and symmetry, including both ground and excited states, unlike, say, the relativistic random phase approximation, which is only applicable to closed-shell systems. Finally, the *R*-matrix method is flexible in that it allows the size of basis sets and the number of interacting channels to be varied. Thus, by increasing the size of these sets in increments, insight is gained as to which are the most important terms, and how convergence is approached.

To consider the photoionization of an $(N+1)$-electron system within an *R*-matrix framework, we start with the wave functions of the states of the *N*-electron final state system (known as target states for historical reasons) [15–17], constructed by introducing a set of (target) states, and possibly pseudostates, Φ_i, that are usually written as a configuration-interaction (CI) expansion in terms of some basis configuration functions ϕ_i,

$$\Phi_i(x_1,x_2,\ldots,x_N) = \sum_k b_{ik}\phi_k(x_1,x_2,\ldots,x_N), \qquad (5)$$

where $x_j = r_j\sigma_j$ represents the spatial and spin coordinates of the j^{th} electron, and the b_{ik} are the ϕ_i configuration mixing coefficients. The configuration functions ϕ_i are constructed from a bound orbital basis set consisting of self-consistent field (SCF) orbitals plus some additional pseudo-orbitals included to model electron correlation effects. For a given ϕ_i configuration function, each one-electron orbital is a product of a radial function, a spherical harmonic, and a spin function. The discrete target states of each ion A^+ (Ti^{4+}, V^{5+}, Cr^{6+}, Mn^{7+}, and Fe^{8+}) orbitals were generated using the code AUTOSTRUCTURE [5–8]. Each of the single-particle spectroscopic orbitals $(1s,2s,2p,3s,3p,3d,4s,4p)$ and the pseudo-orbital $(4\bar{d},4\bar{f},5\bar{s},5\bar{p},5\bar{d})$ radial wave functions was determined using the Thomas-Fermi statistical model radial functions calculated within the program. Using these orbitals, a configuration-interaction (CI) expansion of the target ion A^+ (Ti^{4+}, V^{5+}, Cr^{6+}, Mn^{7+}, and Fe^{8+}) configuration functions to obtain the *N*-electron target state wave function was performed. The set of configuration functions included five spectroscopic configurations, $3s^23p^6$, $3s^23p^53d$, $3s^23p^54s$, $3s^23p^54p$, and $3s3p^63d$, and correlation configurations that, to begin with, included all one- and two-electron replacements of the $n=3$ orbitals of the ground state of ions A^+ (Ti^{4+}, V^{5+}, Cr^{6+}, Mn^{7+}, and Fe^{8+}). To make the subsequent photoionization calculation more tractable, correlation configurations with very small coefficients in the CI expansions were removed, leaving us with 19 correlation configurations. Specifically, the correlation configurations included are $3s^23p^54d$, $3s^23p^54f$, $3s^23p^55s$, $3s^23p^55p$, $3s^23p^55d$, $3s^23p^43d^2$, $3s^23p^43d4p$, $3s^23p^44s4p$, $3s^23p^44p4d$, $3s^23p^43d4f$, $3s^23p^44s4f$, $3s^23p^44p4f$, $3s^23p^33d^3$, $3s^23p^33d^24s$, $3s^23p^34s4p^2$, $3s3p^53d^2$, $3s3p^53d4s$, $3s3p^53d4p$, and $3s3p^43d^3$. Thus, a total of 24 configurations corresponding to 558 *LS* terms were included in the nonrelativistic calculation; for the relativistic (Breit-Pauli) calculation, the relativistic spin-orbit, Darwin, and mass correction terms were added to the Hamiltonian and the resulting CI yielded *LSJ* terms constructed from the *LS* terms.

TABLE I. Calculated (this work and [19]) and experimental (NIST) [18] energy levels in Rydbergs for states of Ti V (Ti^{4+}) relative to the ground state.

Ti V state	J	[19]	This work	Expt.
$3s^23p^6\ {}^1S^e$	0	0.000 00	0.000 00	0.000 00
$3s^23p^53d\ {}^3P^o$	0	2.500 11	2.483 67	2.500 87
	1	2.509 59	2.493 14	2.509 37
	2	2.528 84	2.512 36	2.527 04
$3s^23p^53d\ {}^3F^o$	4	2.612 59	2.611 61	2.617 85
	3	2.631 91	2.627 70	2.634 01
	2	2.650 39	2.643 90	2.649 77
$3s^23p^53d\ {}^1D^o$	2	2.820 21	2.793 07	2.796 44
$3s^23p^53d\ {}^3D^o$	3	2.811 51	2.798 31	2.801 50
	1	2.832 90	2.803 34	2.818 11
	2	2.837 98	2.806 22	2.819 76
$3s^23p^53d\ {}^1F^o$	3	2.850 83	2.828 73	2.837 99
$3s^23p^53d\ {}^1P^o$	1	3.624 50	3.628 58	3.602 42
$3s^23p^54s\ {}^3P^o$	2	3.791 45	3.956 53	3.957 99
	1	3.827 76	3.983 14	3.980 86
	0	3.848 28	4.008 69	4.010 16
$3s^23p^54s\ {}^1P^o$	1	4.005 23	4.064 24	4.043 77

To get some idea of the accuracy of the *N*-electron target state energies, the calculated and experimental (NIST) [18] energy levels relative to the ground state of A^+ (Ti^{4+}, V^{5+}, Cr^{6+}, Mn^{7+}, and Fe^{8+}) states are shown in Tables I–V, and reasonable agreement with experiment is seen. Only for the case of Ti^{4+} is the other theoretical work, that of Nikolić *et al.* [19], and that is also shown in Table I.

Two separate photoionization cross-section calculations were performed for each of the K-like ions (Ti^{3+}, V^{4+}, Cr^{5+}, Mn^{6+}, and Fe^{7+}). In the first, relativistic effects were neglected, and the calculation was carried out with the *LS*-coupling nonrelativistic *R*-matrix codes [8,9,15–17,20,21]. In our *R*-matrix calculations, the final $(N+1)$-electron system continuum wave function is expressed in the form,

$$\begin{aligned}\psi_k(x_1,x_2,\ldots,x_{N+1}) &= A\sum_{ij} c_{ijk}\Phi_i(x_1,\ldots,x_N;\hat{\boldsymbol{r}}_{N+1}\boldsymbol{\sigma}_{N+1})\frac{1}{r_{N+1}}u_{ij}(\boldsymbol{r}_{N+1}) \\ &\quad + \sum_j d_{jk}\boldsymbol{\chi}_j(x_1,\ldots,x_{N+1}), \qquad (6)\end{aligned}$$

TABLE II. Calculated and experimental (NIST) [18] energy levels in Rydbergs for states of V VI (V^{5+}) relative to the ground state.

V VI state	J	This work	Expt.
$3s^23p^6\ ^1S^e$	0	0.000 00	0.000 00
$3s^23p^53d\ ^3P^o$	0	2.781 03	2.808 06
	1	2.793 75	2.819 41
	2	2.819 65	2.842 95
$3s^23p^53d\ ^3F^o$	4	2.939 27	2.941 32
	3	2.959 02	2.961 23
	2	2.980 18	2.981 80
$3s^23p^53d\ ^1D^o$	2	3.135 22	3.145 14
$3s^23p^53d\ ^3D^o$	3	3.137 76	3.148 57
	1	3.158 19	3.179 29
	2	3.163 95	3.174 17
$3s^23p^53d\ ^1F^o$	3	3.189 36	3.195 30
$3s^23p^53d\ ^1P^o$	1	4.095 29	4.059 10
$3s^23p^54s\ ^3P^o$	2	4.963 31	4.978 11
	1	4.995 52	5.005 77
	0	5.032 16	5.046 78
$3s^23p^54s\ ^1P^o$	1	5.071 03	5.081 55

where x_i denote the spatial $\hat{\boldsymbol{r}}_i$ and the spin $\boldsymbol{\sigma}_i$ coordinates of the ith electron, Φ_i are the channel functions obtained by coupling the target state and the angular and spin functions of the continuum electron to form states of the same total angular momentum and parity (and total angular momentum, J, in the Breit-Pauli calculation), and A is the antisymmetrization operator, which takes account of the exchange effects between the target electrons and the free electron. The functions u_{ij} are the single-particle continuum wave functions of the unbound electron, and $\boldsymbol{\chi}_i$ represent the quadratically integrable (L^2) functions, formed from the bound orbitals and included to ensure completeness of the expansion of the total wave function. In the first sum of Eq. (6), only the terms arising from three spectroscopic configurations ($3s^23p^6$, $3s^23p^53d$, and $3s^23p^54s$) are included which abnegates the possibility of pseudoresonances; those three configurations give rise to 9 *LS* terms corresponding to 17 *LSJ* levels (see Tables I–V). In the (purely discrete) second sum, however, all of the terms from the 24 N-electron configurations, coupled to all of the single-particle orbitals, both spectroscopic and correlation, are included in the set of χ_i. The parameters c_{ijk} and d_{jk} are calculated by diagonalizing the $(N+1)$-electron Hamiltonian within the inner region of the R-matrix box.

The initial state wave function, in each case, was constructed from the N-electron target states to include the main configuration, $3s^23p^63d$ or $3s^23p^64s$, along with all single

TABLE III. Calculated and experimental (NIST) [18] energy levels in Rydbergs for states of Cr VII (Cr^{6+}) relative to the ground state.

Cr VII state	J	This work	Expt.
$3s^23p^6\ ^1S^e$	0	0.000 00	0.000 00
$3s^23p^53d\ ^3P^o$	0	3.087 40	3.109 05
	1	3.103 59	3.123 58
	2	3.136 59	3.154 23
$3s^23p^53d\ ^3F^o$	4	3.262 37	3.258 17
	3	3.285 77	3.282 12
	2	3.312 44	3.308 45
$3s^23p^53d\ ^1D^o$	2	3.484 87	3.487 25
$3s^23p^53d\ ^3D^o$	3	3.484 39	3.487 76
	1	3.510 75	3.515 92
	2	3.520 08	3.523 11
$3s^23p^53d\ ^1F^o$	3	3.547 68	3.546 89
$3s^23p^53d\ ^1P^o$	1	4.540 66	4.492 87
$3s^23p^54s\ ^3P^o$	2	6.091 12	6.095 08
	1	6.129 37	6.127 61
	0	6.178 53	6.183 26
$3s^23p^54s\ ^1P^o$	1	6.234 61	6.220 40

TABLE IV. Calculated and experimental (NIST) [18] energy levels in Rydbergs for states of Mn VIII (Mn^{7+}) relative to the ground state.

Mn VIII state	J	This work	Expt.
$3s^23p^6\ ^1S^e$	0	0.000 00	0.000 00
$3s^23p^53d\ ^3P^o$	0	3.388 69	3.405 02
	1	3.408 53	3.423 72
	2	3.448 98	3.462 73
$3s^23p^53d\ ^3F^o$	4	3.577 85	3.579 67
	3	3.606 68	3.598 78
	2	3.640 54	3.631 98
$3s^23p^53d\ ^3D^o$	3	3.824 29	3.821 62
	1	3.860 01	3.857 73
	2	3.873 17	3.869 61
$3s^23p^53d\ ^1D^o$	2	3.831 93	3.825 65
$3s^23p^53d\ ^1F^o$	3	3.903 10	3.895 95
$3s^23p^53d\ ^1P^o$	1	4.982 31	4.913 68
$3s^23p^54s\ ^3P^o$	2	7.321 45	
	1	7.366 32	7.345 72
	0	7.432 03	
$3s^23p^54s\ ^1P^o$	1	7.489 92	7.458 72

TABLE V. Calculated and experimental (NIST) [18] energy levels in Rydbergs for states of Fe IX (Fe^{8+}) relative to the ground state.

Fe IX state	J	This work	Expt.
$3s^23p^6\ ^1S^e$	0	0.000 00	0.000 00
$3s^23p^53d\ ^3P^o$	0	3.679 65	3.697 67
	1	3.704 93	3.720 84
	2	3.756 61	3.769 63
$3s^23p^53d\ ^3F^o$	4	3.889 17	3.880 26
	3	3.920 96	3.912 16
	2	3.962 65	3.953 24
$3s^23p^53d\ ^3D^o$	3	4.154 74	4.151 84
	1	4.199 13	4.197 44
	2	4.219 74	4.215 67
$3s^23p^53d\ ^1D^o$	2	4.167 40	4.162 23
$3s^23p^53d\ ^1F^o$	3	4.253 45	4.244 94
$3s^23p^53d\ ^1P^o$	1	5.394 38	5.326 76
$3s^23p^54s\ ^3P^o$	2	8.621 48	
	1	8.673 25	8.661 59
	0	8.760 97	
$3s^23p^54s\ ^1P^o$	1	8.820 07	8.798 92

TABLE VI. K-like ions (Ti^{3+}, V^{4+}, Cr^{5+}, Mn^{6+}, and Fe^{7+}) states threshold energy in eV compared to experiment [18].

Ions	State	Calculation	Experiment	% Difference
Ti^{3+}	$^2S^e_{1/2}$	33.356	33.300	0.168
	$^2D^e$	43.281	43.243	0.087
	$^2D^e_{3/2}$	43.317	43.267	0.117
	$^2D^e_{5/2}$	43.257	43.220	0.085
V^{4+}	$^2D^e$	65.248	65.242	0.009
	$^2D^e_{3/2}$	65.293	65.281	0.018
	$^2D^e_{5/2}$	65.199	65.204	0.007
Cr^{5+}	$^2D^e$	90.646	90.576	0.077
	$^2D^e_{3/2}$	90.718	90.635	0.091
	$^2D^e_{5/2}$	90.581	90.518	0.069
Mn^{6+}	$^2D^e$	119.118	119.120	0.016
	$^2D^e_{3/2}$	119.218	119.203	0.012
	$^2D^e_{5/2}$	119.027	119.037	0.008
Fe^{7+}	$^2D^e$	151.029	150.956	0.048
	$^2D^e_{3/2}$	151.146	151.070	0.050
	$^2D^e_{5/2}$	150.883	150.843	0.026

electron promotions out the $3s$, $3p$ and the outer shell ($3d$ or $4s$), along with all double promotions of the type $3s^23p^5nln'l'$, and the important double promotions of the $3s^23p^43d^2\ nl$ variety. Other possible two-electron promotions were omitted to ensure that the ground state was not overcorrelated as compared to the target states (i.e., to balance the calculation). The terms arising from these states formed the basis of a large CI calculation to obtain the initial-state wave function. In Table VI are presented the threshold energies of the nonrelativistic states of each of the five K-like ions (Ti^{3+}, V^{4+}, Cr^{5+}, Mn^{6+}, and Fe^{7+}), the $[Ne]3s^23p^63d\ ^2D^e$ state, along with the corresponding two relativistic initial states, the ground state $[Ne]3s^23p^63d\ ^2D^e_{3/2}$ plus the first (metastable) excited state $[Ne]3s^23p^63d\ ^2D^e_{5/2}$. In addition, for the Ti^{3+} ion, we have a third relativistic initial state ($[Ne]3s^23p^64s\ ^2S^e_{1/2}$) that is added to the calculations. Comparing our theoretical ionization potentials with experimental data [18], also shown in the table, it is evident that agreement between theory and experiment is rather good.

Since this work concerns K-like ions (Ti^{3+}, V^{4+}, Cr^{5+}, Mn^{6+}, and Fe^{7+}), it is of interest to see how the energy gap (fine structure splitting) between $^2D^e_{3/2}$ and $^2D^e_{5/2}$ levels changes as the nuclear charge Z of those ions increases along the sequence. In Table VII, we present a comparison between calculated and experimental [18] fine structure splitting (energy gap) corresponding to the two relativistic levels $^2D^e_{3/2}$ and $^2D^e_{5/2}$.

In both *LS* and Breit-Pauli calculations, the R-matrix box radii were 17.64 a.u. for Ti^{3+}, 15.45 a.u. for V^{4+}, 12.80 a.u. for Cr^{5+}, 11.35 a.u. for Mn^{6+}, and 9.25 a.u. for Fe^{7+}, and 34 basis orbitals were used to represent the continuum for each value of the angular momentum.

The QB method [10–12] is adopted in this work to determine the resonance energies and widths. The QB method works in the *R*-matrix environment; the reactance matrix K is computed by matching the inner-region radial functions to $n \times n_0$ linear combinations of the outer-region radial functions for n_0 open channels (n is the total number of channels retained in the close-coupling expansion). Diagonalizing the K matrix in open-channel space leads to K_{00}, with eigenvalues λ_i; the eigenphase for each channel is given by

$$\delta_i = \tan^{-1}\lambda_i, \quad i = 1, n_0, \tag{7}$$

and the sum over all channels gives the eigenphase sum δ. The resonance position is computed as the energy of the maximum gradient $d\delta/dE = \delta'$.

To calculate the resonance width with the QB method, we consider the Breit-Wigner [22] form of the eigenphase sum,

$$\delta(E) = \bar{\delta}(E) + \tan^{-1}\frac{\Gamma/2}{E_r - E'}, \tag{8}$$

where E_r is the resonance energy, Γ is the resonance width, and $\bar{\delta}$ is the background eigenphase. Differentiating, evaluating at $E = E_r$, and assuming the background varies slowly over the resonance profile, that is, $\bar{\delta}' \ll \Gamma^{-1}$, we get the width as

$$\Gamma = 2/\delta'(E_r), \tag{9}$$

which means at resonance the width is related to the inverse of the eigenphase derivative.

TABLE VII. Calculated and experimental [18] fine structure splitting ΔE (eV) between $^2D^e_{3/2}$ and $^2D^e_{5/2}$ levels for K-like ions Sc^{2+} [36], Ti^{3+}, V^{4+}, Cr^{5+}, Mn^{6+}, and Fe^{7+}.

Ions	Z	Calculated ΔE	Experimental ΔE
Sc^{2+} [36]	21	0.030	0.024
Ti^{3+}	22	0.060	0.047
V^{4+}	23	0.094	0.077
Cr^{5+}	24	0.137	0.117
Mn^{6+}	25	0.191	0.166
Fe^{7+}	26	0.263	0.227

III. RESULTS AND DISCUSSION

Among ions of the potassium isoelectronic sequence studied in this work, the Ti^{3+} is the most extensively investigated experimentally and theoretically [4,13,14,19,23–25] because of the presence, in the photoionization cross-section spectra, of the giant ($3p \rightarrow 3d$ excitation) resonances; in consequence we first report on the photoionization cross sections of Ti^{3+} with nonrelativistic and relativistic calculations. In the nonrelativistic calculations of Ti^{3+} ions, the initial states of this ion considered are the ground $[Ne]3s^23p^63d\ ^2D^e$ and the first excited $[Ne]3s^23p^64s\ ^2S^e$ states. In Figs. 1 and 2, we present results of the nonrelativistic calculations for both initial states for photon energy from the $3d$ ionization threshold (43.28 eV) to 83.0 eV; Fig. 1 shows the photoionization cross sections from threshold to 51.0 eV while Fig. 2 goes from about 51.0 to 83 eV; since, in both cases, the photoionization cross sections obtained using length and velocity forms agree very well, only one form (length) is displayed here and in all subsequent figures.

In the Ti^{3+} excited $^2S^e$ state, the $4s$ electron ionization (33.35 eV) threshold cross section [not seen in Fig. 1(a)] is 0.695 Mb. For photon energy below 45.0 eV [Fig. 1(a)], there are no resonances in the excited $^2S^e$ state photoionization cross section; only the direct photoionization process is possible here

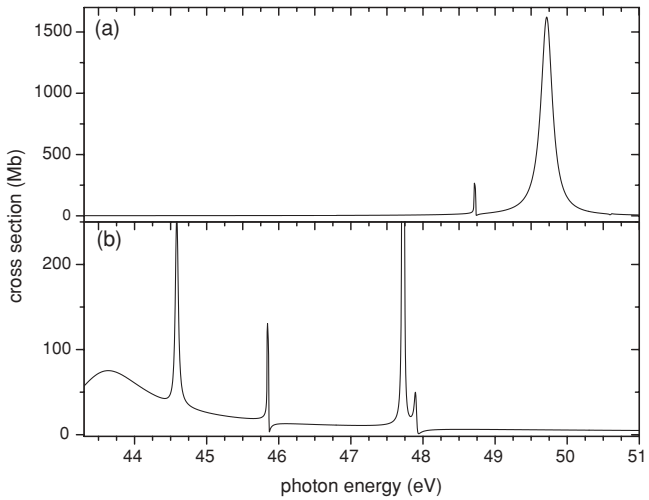

FIG. 1. Calculated nonrelativistic photoionization cross sections of Ti^{3+} from threshold to 51.0 eV: (a) initial $^2S^e$ excited state showing the strongest resonance $^2S^e \rightarrow (3p^5 3d\ ^1P)4s\ ^2P^o$ at energy 49.09 eV, and (b) initial $^2D^e$ ground state showing the strongest resonance $^2D^e \rightarrow 3p^5(3d^2\ ^3F)\ ^2F^o$ at energy 43.64 eV. Note the truncation in resonance structure at threshold in (b).

and leads to a $[(3s^2 3p^6\ ^1S^e)\ \varepsilon p]\ ^2P^o$ final state of the $(N+1)$-electron system. Above 45.0 eV, we enter the $3p$ electron excitation region characterized by the presence of series of Rydberg resonances associated with $3p$ photoexcitation [Figs. 1(a) and 2(a)]; these series of Rydberg resonances are characterized as $[(3p^5\ nd)4s\ ^2P^o]$ and $[(3p^5 n's)\ 4s\ ^2P^o]$. These two sequences of Rydberg resonances dominate the Ti^{3+} excited $^2S^e$ state photoionization cross-section spectrum [Fig. 1(a)]. Among these resonances we note the resonance located at 48.62 eV (18.5 meV width), attributed to transition $^2S^e \rightarrow 3p^5(4s^2\ ^1S)$ $^2P^o$ and the remarkably large and broad resonance feature in Fig. 1(a) at 49.09 eV (186.4-meV width); this peak reaches 1556 Mb and is attributed to transition $^2S^e \rightarrow (3p^5 3d\ ^1P)4s\ ^2P^o$ that is followed by autoionization (decay) to the ground $3s^2 3p^6\ ^1S^e$ state of Ti^{4+}. Figure 2(a) displays higher order members of those Rydberg series of resonances originating from $3p$ electron photoexcitation to higher principal quantum number $[(3p^5\ nd)\ 4s\ ^2P^o]$ and $[(3p^5 n's)\ 4s\ ^2P^o]$ with $n \geqslant 4$ and $n' \geqslant 5$. They are mixed and decay to the $[(3s^2 3p^6\ ^1S^e)\ \varepsilon p\ ^2P^o]$ continuum. The limit of those two sequences is the excited target Ti^{4+} $(3p^5 4s\ ^1P^o)$ state at energy 98.55 eV (98.23 eV from experiment [18]). Due to dipole transition selection rules, only the transition $^2S^e \rightarrow\ ^2P^o$ is allowed; this confers to the outer $4s$ electron, in this photoionization of Ti^{3+} excited $^2S^e$ state case, the role of "spectator" since it only contributes to angular momentum coupling with its spin. The very limited number of resonances (only one strong peak) observed in this case is illustrative of this fact.

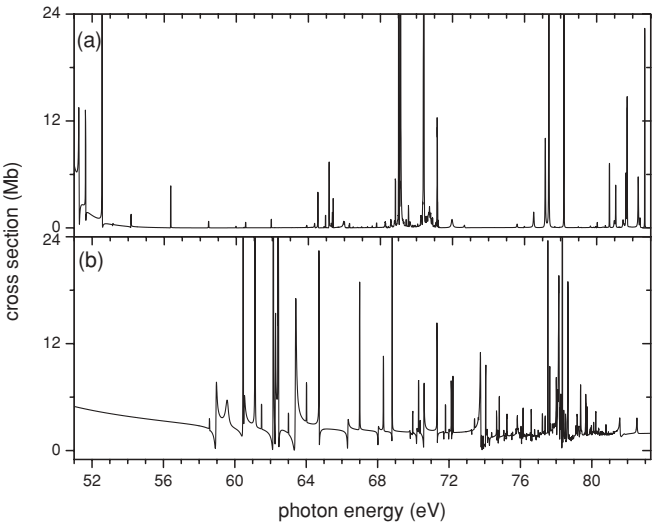

FIG. 2. Calculated nonrelativistic photoionization cross sections of Ti^{3+} from 51.0 to 83.0 eV: (a) initial $^2S^e$ excited state showing the Rydberg series of resonances $[(3p^5\ nd)\ 4s\ ^2P^o]$ and $[(3p^5 n's)\ 4s\ ^2P^o]$ with $n \geqslant 4$ and $n' \geqslant 5$ and (b) initial $^2D^e$ ground state showing series of Rydberg resonances $[(3p^5\ nd)\ 3d\ ^2P^o, {}^2F^o]$ and $[(3p^5 n's^3P^o)\ 3d\ ^2P^o, {}^2F^o]$ with $n \geqslant 4$ and $n' \geqslant 5$.

For the ground $^2D^e$ state of Ti^{3+}, the photoionization cross sections in Figs. 1(b) and 2(b) exhibit far more complex structure than the excited $^2S^e$ state. At threshold (43.28 eV), the cross section is 56.0 Mb [Fig. 1(b)]; for photon energy in the vicinity of the threshold the cross section is a mixture of direct nonresonant and indirect resonance processes, and it is evident that the resonance excitations are dominant in this region where the cross section can reach hundreds of Mb. For photon energy up to 51 eV [Fig. 1(b)], the cross section is dominated by giant, $3p \rightarrow 3d$ resonances; these $3p \rightarrow 3d$ resonances are so strong because they represent $\Delta n = 0$ transitions, and, since the spatial extent of a wave function is determined largely by the principal quantum number, n, the $3p$ and $3d$ wave functions occupy substantially the same region of space, resulting in significant overlap and a rather large dipole matrix element. The photoionization cross section in this region is dominated by resonances which decay via autoionizing processes leading to the ground $3s^2 3p^6\ ^1S^e$ state of Ti^{4+}. In this region, the direct photoionization contribution to the cross section is quite small; thus the giant resonances are fairly symmetric since any asymmetry is due to interference between the resonant and nonresonant amplitudes. The direct photoionization cross section for the outer $3d$ electron, has been calculated [26] for Ti^{3+} at 45 eV to be 2.2 Mb, more than an order of magnitude smaller than the present result for the total (direct and indirect photoionization cross sections) of about 27.0 Mb (30.0 Mb experimentally [13]). Among the most prominent resonances in Fig. 1(b) is the resonance at the threshold (located at 43.64 eV with a width of 1.27 eV), identified as the $^2D^e \rightarrow 3p^5(3d^2\ ^3F\ ^2F^o$ transition, the resonance at 44.59 eV (41.8-meV width) identified $^2D^e \rightarrow (3p^5 3d\ ^3P)4s\ ^2P^o$ and the resonance at 47.733 eV (5.9-meV width) attributed to $^2D^e \rightarrow 3p^5(3d^2\ ^3P)$ $^2P^o$. In fact, those giant resonances [Fig. 1(b)] are the dominant resonances originating from $3p$ photoexcitation; they are the lowest members of the series of Rydberg resonances that start from the threshold and continue to the higher energy region [Fig. 2(b)] with higher principal quantum number. Examples of the higher members of these series of Rydberg resonance, $[(3p^5\ nd)\ 3d\ ^2P^o, {}^2F^o]$ and $[(3p^5 n's^3P^o)\ 3d\ ^2P^o, {}^2F^o]$ with $n \geqslant 3$ and $n' \geqslant 4$ are displayed in both Figs. 1(b) and 2(b).

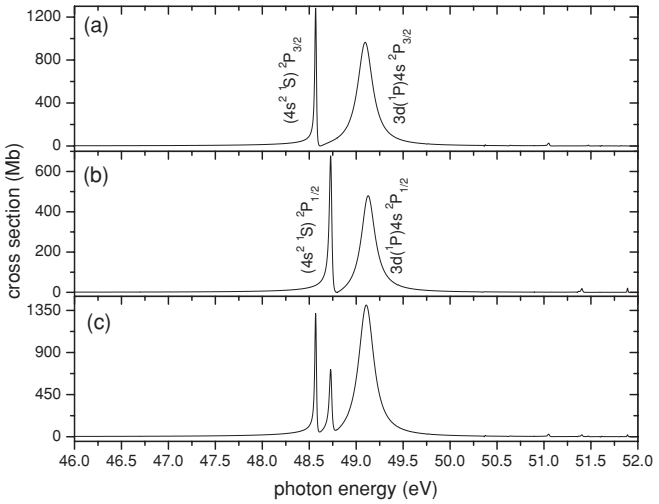

FIG. 3. Calculated Breit-Pauli (relativistic) photoionization cross sections of the excited $^2S^e_{1/2}$ state of Ti^{3+} from 46.0 to 52.0 eV showing (a) the partial cross section to the $j = 3/2$ final state, (b) the partial cross section to the $j = 1/2$ final state, and (c) the total $^2S^e_{1/2}$ cross section, dominated by the resonance at 49.09 eV. For simplicity $3p^5$ is omitted from each of the resonance designations.

The series of Rydberg resonances interfere with direct photoionization continua $3s^23p^6\ ^1S^e$ $(\varepsilon f, \varepsilon p)$, and converge to the six Ti^{4+} $3s^23p^53d$ thresholds starting with $^3P^o$ at a photon energy of 77.16 eV to $^1P^o$ at 92.62 eV (92.23 eV from experiment [18]). In the region above 77.16 eV [Fig. 2(b)], the photon energy is high enough to produce, through resonance excitation followed by autoionization, both ground and excited states of Ti^{4+} including $3s^23p^6\ ^1S^e$, $3s^23p^53d\ ^3P^o$, $3s^23p^53d\ ^3F^o$, etc., that is, ionization plus excitation; the continuum cross sections (direct process) comprise $3s^23p^6\ ^1S^e$ $(\varepsilon f, \varepsilon p)$, $3s^23p^53d\ ^3P^o$ $(\varepsilon d, \varepsilon s)$, $3s^23p^53d\ ^3F^o$ $(\varepsilon d, \varepsilon s)$ and so forth.

With the introduction of the spin-orbit interaction in our calculations with the use of the Breit-Pauli R-matrix method, initial states of the Ti^{3+}ion are represented by the ground $[Ne]3s^23p^63d\ ^2D^e_{3/2}$ state, the first excited $[Ne]3s^23p^63d\ ^2D^e_{5/2}$ state and the second excited $[Ne]3s^23p^64s\ ^2S^e_{1/2}$ state. The calculated relativistic (Breit-Pauli) cross sections for the photoionization of Ti^{3+} in the excited $^2S^e_{1/2}$ initial state is shown in Fig. 3. The individual $^2S^e_{1/2} \rightarrow\ ^2P^o_{3/2}$ and $^2S^e_{1/2} \rightarrow\ ^2P^o_{1/2}$ cross sections are presented in Figs. 3(a) and 3(b), respectively, while the total is given in Fig. 3(c).

As in the nonrelativistic case, the photoionization cross section is dominated by autoionizing resonances. Among important resonances in Fig. 3 note the very narrow resonances due to transitions $^2S^e_{1/2} \rightarrow 3p^5(4s^2\ ^1S)\ ^2P^o_{3/2}$ [Fig. 3(a)] and $^2S^e_{1/2} \rightarrow 3p^5(4s^2\ ^1S)\ ^2P^o_{1/2}$ [Fig. 3(b)] located at 48.57 eV (15.2-meV width) and 48.73 eV (26.9-meV width), respectively. Both resonances arise from the splitting of LS resonance shown in Fig. 1(a) at 48.62 eV (see above), identified in LS coupling as $^2S^e \rightarrow 3p^5(4s^2\ ^1S)\ ^2P^o$. Dominating the $^2S^e_{1/2}$ cross section, however, are clearly the giant $3p \rightarrow 3d$ resonances identified as $^2S^e_{1/2} \rightarrow (3p^53d\ ^1P)4s\ ^2P^o_{3/2}$ in Fig. 3(a) and $^2S^e_{1/2} \rightarrow (3p^53d\ ^1P)4s\ ^2P^o_{1/2}$ in Fig. 3(b); their positions and widths are 49.09 eV and 192.7 meV, and 49.12 eV and 175.2 meV, respectively. Although the relativistic interactions cause a splitting of these two resonances, the splitting is so much smaller than the widths so that the splitting is unobservable. In the experiment conducted by Schippers *et al.* [13] on the photoionization of Ti^{3+}, the excited $^2S^e_{1/2}$ state was not part of the target beam because it is significantly excited (by 9.96 eV) compared to the ground $^2D^e_{3/2}$ state, while in the case of Sc^{2+} the $^2S^e_{1/2}$ state was part of the target beam because it is only 3.16 eV above the ground $^2D^e_{3/2}$ state [27,28]. In the experiment on the photoionization of Ti^{3+} reported by Ryabtsev *et al.* [14], however, the excited $^2S^e_{1/2}$ state was included as part of the target. From this experiment, resonances, originating from transitions $^2S^e_{1/2} \rightarrow 3p^5(4s^2\ ^1S)\ ^2P^o_{3/2}$ [Fig. 3(a)] and $^2S^e_{1/2} \rightarrow 3p^5(4s^2\ ^1S)\ ^2P^o_{1/2}$ [Fig. 3(b)], were found at 48.64 and 48.69 eV (24.8-meV width for each of them), respectively; it is clear that our theoretical results (48 55 and 48.73 eV) are in rather good agreement with the experimental data from Ryabtsev *et al.* [14] for those particular resonances. For the strongest and broadest resonance feature in the excited $Ti^{3+2}S^e$ state photoionization cross section, the two spin-orbit components of the $^2S^e \rightarrow (3p^53d\ ^1P)4s\ ^2P^o$, there are no experimental or previous theoretical results with which to compare. However, we can say that both resonances are just equivalent to one single resonance attributed to transition $^2S^e \rightarrow (3p^53d\ ^1P)4s\ ^2P^o$, and this resonance was observed in the photoionization of the ground $[Ne]3s^23p^64s\ ^2S^e_{1/2}$ state of Ca^+ [4,29–35] and in the excited $[Ne]3s^23p^64s\ ^2S^e_{1/2}$ state of Sc^{+2} [4,27,28,36,37], and in each of those cases, this resonance is very broad and strong with respective positions 33.19 and 41.80 eV (experimental data [4,13]). Consequently, from Ca^+ to Sc^{2+}, this resonance position, compared to the 4s ionization threshold (11.87 eV in Ca^+ and 21.59 eV in Sc^{2+}), changes from 21.32 to 20.21 eV [4,13]. This tendency in the resonance position to get closer and closer to the 4s electron threshold, as the nuclear charge Z increases, should continue with Ti^{3+} and higher Z potassiumlike ions; our theoretical calculation places it at 15.74 eV from the 4s ionization threshold (33.35 eV). The width of this resonance, on the contrary, increases from Ca^+ to Sc^{2+} (92.0 and 147 meV, respectively); our calculated width is 193.0 meV, which is in agreement with the trend in resonance width to augment as the nuclear charge Z of those ions increases. In addition, this strong $^2S^e \rightarrow (3p^53d\ ^1P)4s\ ^2P^o$ transition has an oscillator strength [38,39] in our calculation of 2.17 out of a total oscillator strength for 3p photoabsorption of 6 (i.e., this transition accounts for about 36.17% of the total 3p oscillator strength, an enormous contribution).

The Breit-Pauli results for the photoionization of the ground $^2D^e_{3/2}$ state of Ti^{3+} are presented in Fig. 4. Note that, in the relativistic realm, L is no longer a good quantum number so that the final states of the system, the Ti^{4+} ion plus photoelectron, can be characterized only by total angular momentum, j, strictly speaking. Thus, from the $^2D^e_{3/2}$ ground state, transitions to final states with $j = 5/2$, $3/2$, and $1/2$ are allowed, and these cross sections are shown in Figs. 4(a)–4(c), respectively; the total $^2D^e_{3/2}$ photoionization cross section is shown in Fig. 4(d). For photon energy between the 3d ionization threshold (43.31 eV) and 49.50 eV, resonances are seen to dominate the cross section, although the direct nonresonant photoionization channel is strong enough for interference to

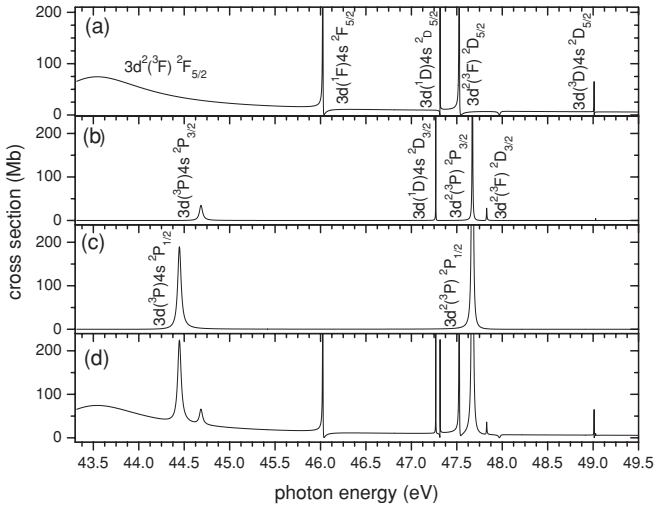

FIG. 4. Calculated Breit-Pauli (relativistic) photoionization cross sections of the ground $^2D^e_{3/2}$ state of Ti^{3+} showing (a) the partial cross section to the $j = 5/2$ final state, (b) the partial cross section to the $j = 3/2$ final state, (c) the partial cross section to the $j = 1/2$ final state, and (d) the total $^2D^e_{3/2}$ cross section, dominated by the $3p^5(3d^2\ ^3F)\ ^2F^o_{5/2}$ resonance at 43.54 eV. For simplicity $3p^5$ is omitted from each of the resonance designations.

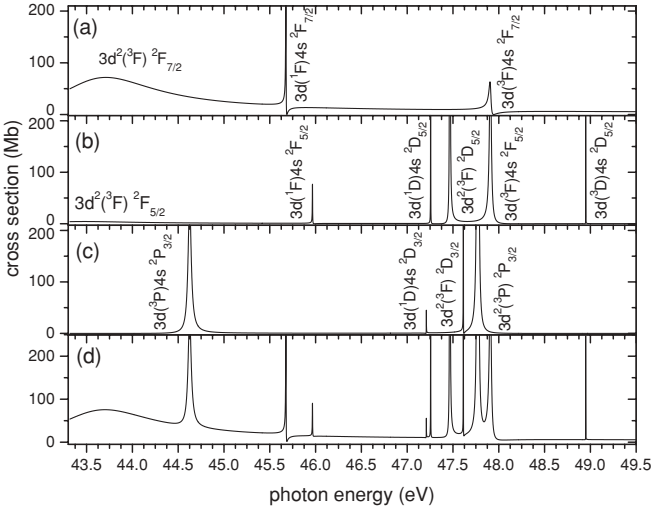

FIG. 5. Calculated Breit-Pauli (relativistic) photoionization cross sections of the excited $^2D^e_{5/2}$ state of Ti^{3+} showing (a) the partial cross section to the $j = 7/2$ final state, (b) the partial cross section to the $j = 5/2$ final state, (c) the partial cross section to the $j = 3/2$ final state, and (d) the total $^2D^e_{5/2}$ cross section, dominated by the $3p^5(3d^2\ ^3F)\ ^2F^o_{7/2}$ resonance at 43.71 eV. For simplicity $3p^5$ is omitted from each of the resonance designations.

occur and produce the asymmetric line shapes, Fano profiles, observed in the cross sections [Figs. 4(a) and 4(d)]. The most prominent resonance is located at 43.544 eV with 1.28 eV width, and it is due to the $^2D^e_{3/2} \rightarrow 3p^5(3d^2\ ^3F)\ ^2F^o_{5/2}$ transition, a $\Delta j = 1$ transition. This resonance decays via a super-Coster-Kronig transition ($3p^5 3d^2 \rightarrow 3p^6 + e^-$) that is also observed in the photoionization cross sections of the excited (metastable) $[Ne]3s^2 3p^6 3d\ ^2D^e$ states of Ca^+ [4,29–35] and the ground $[Ne]3s^2 3p^6 3d\ ^2D^e$ state of Sc^{2+} [4,27,28,36,37]; as long as the excitation energy of this resonance is above the $3d$ threshold, this channel is open and results in this broad giant resonance. When the excitation energy is below the $3d$ ionization threshold, this decay channel is closed, and this is the case for K-like higher Z ions starting with V^{4+} (see below). Our theoretical results show good agreement with experimental data [13] that places this resonance at 43.460 eV with 1.5 eV width. We note that, compared to the $3d$ ionization threshold, the experimental positions of this resonance are [4,36] 19.16 eV in metastable Ca^+, 12.38 eV in ground state Sc^{2+}, and 0.22 eV in Ti^{3+}; our calculations ([35,36] and this work) show it at positions 19.17, 12.44, and 0.31 eV, respectively, which is rather good agreement. Other important resonances in the photoionization $^2D^e_{3/2}$ state of Ti^{3+} include the $^2D^e_{3/2} \rightarrow (3p^5 3d\ ^3P)4s\ ^2P^o_{1/2}$ ($\Delta j = -1$) located at 44.453 eV (44.4 meV width), seen in Fig. 4(c), and the $^2D^e_{3/2} \rightarrow (3p^5 3d\ ^3P)4s\ ^2P^o_{3/2}$ ($\Delta j = 0$) resonance at 44.688 eV (40.4 meV width), seen in Fig. 4(b). Note the weakness of the $^2P^o_{3/2}$ resonance in terms of strength and width compared to the $^2P^o_{1/2}$ resonance. Additional resonances resulting from $^2D^e_{3/2}$ photoionization include $^2D^e_{3/2} \rightarrow 3p^5(3d^2\ ^3P)\ ^2P^o_{1/2}$ at 47.681 eV (4.3 meV width) shown in Fig. 4(c), $^2D^e_{3/2} \rightarrow 3p^5(3d^2\ ^3P)\ ^2P^o_{3/2}$ at 47.676 eV (6.1 meV width) seen in Fig. 4(b), $^2D^e_{3/2} \rightarrow 3p^5(3d^2\ ^3F)\ ^2D^o_{5/2}$ located at 47.531 eV (1.4 meV width) in Fig. 4(a), and $^2D^e_{3/2} \rightarrow (3p^5 3d\ ^3F)4s\ ^2F^o_{5/2}$ at 46.030 eV (3.5 meV width) in Fig. 4(a). Note that the $^2D^e \rightarrow {}^2D^o$ photoionizing transitions are forbidden in this energy range without the introduction of relativistic effects; there is no $^2D^o$ continuum since the ionization of the $3d$ electron leads only to ^2P and ^2F continua.

In Fig. 5, the calculated Breit-Pauli results are presented for the corresponding photoionization cross section for the excited $^2D^e_{5/2}$ state, for photon energy from threshold to 49.50 eV, and the partial cross sections for $j = 7/2$, $5/2$, and $3/2$ final states are shown in Figs. 5(a)–5(c), respectively. The total photoionization cross section for the $^2D^e_{5/2}$ initial state is shown in Fig. 5(d). The strongest resonance, located at 43.718 eV [Fig. 5(a)], $^2D^e_{5/2} \rightarrow 3p^5(3d^2\ ^3F)\ ^2F^o_{7/2}$, has a width of 1.3 eV (1.5 eV experimentally); it is of substantially the same width as the corresponding $^2D^e_{3/2}$ resonance (1.28 eV) at 43.544 eV [Fig. 4(a)]. Most resonances seen in Fig. 5 for the $Ti^{3+2}D^e_{5/2}$ cross sections have their equivalent already listed in the case of $Ti^{3+2}D^e_{3/2}$ discussed previously; among them are $^2D^e_{5/2} \rightarrow 3p^5(3d^2\ ^3F)\ ^2F^o_{5/2}$ at 43.484 eV [Fig. 5(b)] with $\Delta j = 0$, $^2D^e_{5/2} \rightarrow (3p^5 3d\ ^3P)4s\ ^2P^o_{3/2}$ ($\Delta j = -1$) located at 44.628 eV [Fig. 5(c)], and $^2D^e_{5/2} \rightarrow 3p^5(3d^2\ ^3P)\ ^2P^o_{3/2}$ at 47.616 eV [Fig. 5(c)]. Another example of $\Delta j = 0$ but with $\Delta L = 0$, $^2D^e_{5/2} \rightarrow 3p^5(3d^2\ ^3F)\ ^2D^o_{5/2}$ is seen in Fig. 5(b) at 47.471 eV. Furthermore, there are $^2D^e_{5/2} \rightarrow (3p^5 3d\ ^1F)4s\ ^2F^o_{5/2}$ at 47.917 eV (23.7-meV width) [Fig. 5(b)] and $^2D^e_{5/2} \rightarrow (3p^5 3d^1F)4s\ ^2F^o_{7/2}$ at 47.910 eV [Fig. 5(a)] (26.3-meV width). The fine structure splitting between the $^2D^e_{3/2}$ and $^2D^e_{5/2}$ states of Ti $^{+3}$ ions, which is calculated to be $\Delta E = 0.060$ eV (experimental value is 0.047 eV [13,18]), is mirrored in the various resonance energy differences: $^2D^e_{3/2} \rightarrow 3p^5(3d^2\ ^3F)\ ^2F^o_{5/2}$ at 43.544 eV in Fig. 4(a) and $^2D^e_{5/2} \rightarrow 3p^5(3d^2\ ^3F)$

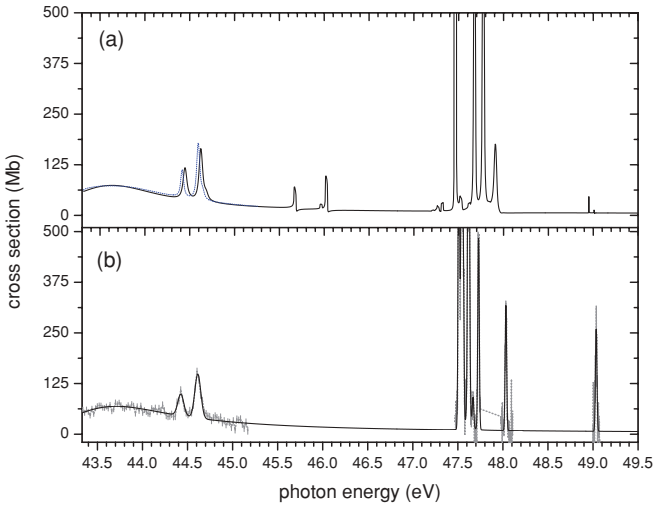

FIG. 6. (Color online) Ti^{3+} photoionization cross sections from 43.30 to 49.50 eV for a weighted average of $^2D^e_{3/2}$ and $^2D^e_{5/2}$ initial states; (a) theoretical calculations showing Nikolić *et al.* [19] results (blue short dots) and results from this work (black solid line), and (b) experiment [13] showing measured cross-section data (gray short dots) with error bars (low-energy region) and the result of a resonance fit comprising 11 individual resonances (solid line). Note the cutoff, at threshold, of the giant $3p^5(3d^2\ ^3F)\ ^2F^o$ dipole resonance in panels (a) and (b). The dotted curve in the upper panel is the theoretical result of Ref. [19].

$^2F^o_{5/2}$ at 43.488 eV in Fig. 5(b); $^2D^e_{3/2} \rightarrow (3p^5 3d\ ^3P)4s\ ^2P^o_{3/2}$ at 44.688 eV in Fig. 4(b) and $^2D^e_{5/2} \rightarrow (3p^5 3d\ ^3P)4s\ ^2P^o_{3/2}$ at 44.628 eV in Fig. 5(c); and $^2D^e_{3/2} \rightarrow 3p^5(3d^2\ ^3P)\ ^2P^o_{3/2}$ at 47.676 eV in Fig. 4(b) and $^2D^e_{5/2} \rightarrow 3p^5(3d^2\ ^3P)\ ^2P^o_{3/2}$ at 47.616 eV in Fig. 5(c).

The experimental Ti^{3+} ion beam [13] consisted of two components: 45.0% $^2D^e_{3/2}$ and 55.0% $^2D^e_{5/2}$, and these fractions are used to obtain the theoretical total photoionization cross section for Ti^{3+} for a meaningful comparison with experiment [13] shown in Fig. 6. The experimental photon energy range is from the $3d$ ionization threshold to 49.50 eV; this means the experiment [13] only involves the region of giant resonances. Those resonances, originating from $3p \rightarrow 3d$ and $3p \rightarrow 4s$ excitations, have been investigated theoretically and experimentally [3,4,13,14,19,23–25,27–37]. In Fig. 6, it is seen that the main feature of both theoretical and experimental cross sections is the strongest and broadest resonance at the threshold, which is the giant dipole transition $^2D^e \rightarrow 3p^5(3d^2\ ^3F)\ ^2F^o$. Despite the fact that this resonance is truncated (some of it is below the ionization threshold), it is still stronger than what was observed in excited (metastable) Ca^+ [4,13] and ground state of Sc^{2+} [4,13]. The width of this resonance is 1.5 eV experimentally [13,14] (1.3 eV in the present work), while for the metastable state of Ca^+ and the ground state of Sc^{2+}, corresponding widths are 0.324 and 0.847 eV, respectively [4,13]. The loss of strength in this resonance in Ti^{3+}, due to truncation at the threshold, was estimated by Ryabtsev *et al.* [14] to be about 40%.

Comparing our theoretical results and experimental data, shown in Fig. 6, good agreement between them is seen. For example, the calculation for the large resonance at threshold exhibits a maximum of 74.04 Mb at 43.62 eV, while from experiment [13] the maximum is 68.86 Mb at 43.70 eV, quite good agreement indeed and well within the experimental uncertainty of 15%. Another illustration of the good agreement between theory (this work) and experiment [13] are the two narrower resonance structures that are superimposed on the giant resonance located theoretically at 44.45 and 44.62 eV [Fig. 6(a)], while the experiment [13] placed them at 44.42 and 44.61 eV, respectively [Fig. 6(b)]. Despite this good agreement in the low-energy region between the present work and experiment [13] (Fig. 6), very small differences between theory [Fig. 6(a)] and experiment [Fig. 6(b)] are seen in the 47.50–47 eV photon energy region, in terms of resonance positions, where the largest deviation observed is 0.16 eV only. Another less important difference between theory (this work) and experimental data [13] shown in Fig. 6(b) is the fact that cross-section measurements were not performed in the energy ranges 45.1685–47.4667 eV, 47.7484–47.9757 eV, and 48.1085–48.9978 eV. This explains why, in the photon energy region from 45.6 to 46.1 eV, the two small resonance features seen at 45.68 and 46.03 eV (with respective widths 3.8 and 3.4 meV) in Fig. 6(a) were not part of experimental [13] results [Fig. 6(b)]. However, the experiment of Ryabtsev *et al.* [14] showed similar resonance features with almost the same widths (4.3 and 3.7 meV), but there are deviations in the resonance positions (see Table VIII below) compared to our results. Also shown in Fig. 6 are the theoretical results of Ref. [19] which show excellent agreement with the present results; these cross sections were only reported for the first 2 eV above threshold, however. Another recent calculation [25] in the same 2-eV region (not shown) shows very similar agreement.

A very useful check upon the magnitude of photoionization cross sections is the Thomas-Reiche-Kuhn sum rule [38] which states that the sum of the oscillator strengths (integral over the continuum part) to all possible final states from a given initial state of an atom or atomic ion is equal to the number of electrons in the initial state. It has also been found that the sum rule is true to an excellent approximation subshell by subshell [39]. Since the photoionization cross section is simply a multiplicative constant times the (differential) oscillator strength [39], the total oscillator strength represented by the photoionization cross section can be easily calculated. In the present case, it is expected that the cross section should include almost all of the oscillator strength from the $3p^6$ subshell owing to the giant $3p \rightarrow 3d$ resonances which all occur in the continuum; for the outer shell electron, on the other hand, most of the oscillator strength likely contributes in the discrete spectrum, thus representing photoexcitation rather than photoionization. The theoretical oscillator strength sum for Ti^{3+} within the experimental [13] photon energy range (from threshold to 49.5 eV), is found to be 2.81 out of possible 6 (the number of $3p$ electrons); the measured oscillator strength is 2.631, in quite good agreement with theory. The theoretical and experimental results, respectively, represent about 47.0% and 44.0% of the total $3p$ oscillator strength, and the photon energy range is from threshold to 49.5 eV (6.2-eV wide); through those considerations, we confirm the important contribution of those giant dipole resonances to the sum of oscillator strengths in the photoionization of Ti^{3+}.

TABLE VIII. Ti^{3+} theoretical (relativistic Breit-Pauli) and experimental [13,14] resonance energies E_{res} (eV), widths Γ(meV), and the corresponding transition designations.

This calculation		Transitions	Experiment		
E_{res}	Γ		E_{res} [14]	Γ [14]	E_{res} [13]
43.54	1280	$^2D^e_{3/2} \rightarrow 3p^5(3d^2\ ^3F)\ ^2F^o_{5/2}$	43.67	930.9	43.46
43.71	1300	$^2D^e_{5/2} \rightarrow 3p^5(3d^2\ ^3F)\ ^2F^o_{7/2}$	43.67	930.9	
43.48	1280	$^2D^e_{5/2} \rightarrow 3p^5(3d^2\ ^3F)\ ^2F^o_{5/2}$			
44.45	44.4	$^2D^e_{5/2} \rightarrow (3p^5 3d\ ^3P)4s\ ^2P^o_{1/2}$	44.46	39.7	44.42
44.62	40.4	$^2D^e_{5/2} \rightarrow (3p^5 3d\ ^3P)4s\ ^2P^o_{3/2}$	44.65	52.1	44.61
44.68	40.4	$^2D^e_{3/2} \rightarrow (3p^5 3d\ ^3P)4s\ ^2P^o_{3/2}$			
45.68	3.8	$^2D^e_{5/2} \rightarrow (3p^5 3d\ ^3F)4s\ ^2F^o_{7/2}$	46.04	4.3	
45.97	3.4	$^2D^e_{5/2} \rightarrow (3p^5 3d\ ^3F)4s\ ^2F^o_{5/2}$	46.33	4.7	
46.03	3.4	$^2D^e_{3/2} \rightarrow (3p^5 3d\ ^3F)4s\ ^2F^o_{5/2}$	46.38	4.7	
47.46	1.4	$^2D^e_{5/2} \rightarrow 3p^5(3d^2\ ^3F)\ ^2D^o_{5/2}$	47.77		47.62
47.52	1.4	$^2D^e_{3/2} \rightarrow 3p^5(3d^2\ ^3F)\ ^2D^o_{5/2}$	47.81		47.67
47.68	6.1	$^2D^e_{3/2} \rightarrow 3p^5(3d^2\ ^3P)\ ^2P^o_{1/2}$	47.58	16.1	47.54
47.61	4.3	$^2D^e_{5/2} \rightarrow 3p^5(3d^2\ ^3P)\ ^2P^o_{3/2}$	47.66	23.6	47.51
47.66	4.3	$^2D^e_{3/2} \rightarrow 3p^5(3d^2\ ^3P)\ ^2P^o_{3/2}$	47.71	9.9	47.56
47.91	26.3	$^2D^e_{5/2} \rightarrow (3p^5 3d\ ^1F)4s\ ^2F^o_{7/2}$	48.37	28.5	
47.91	23.7	$^2D^e_{5/2} \rightarrow (3p^5 3d\ ^1F)4s\ ^2F^o_{5/2}$	48.32	18.6	
48.57	15.2	$^2S^e_{1/2} \rightarrow 3p^5(4s^2\ ^1S)\ ^2P^o_{3/2}$	48.64	24.8	
48.73	26.9	$^2S^e_{1/2} \rightarrow 3p^5(4s^2\ ^1S)\ ^2P^o_{1/2}$	48.69	24.8	
49.04	192.7	$^2S^e_{1/2} \rightarrow (3p^5 3d\ ^1P)4s\ ^2P^o_{3/2}$			
49.12	175.2	$^2S^e_{1/2} \rightarrow (3p^5 3d\ ^1P)4s\ ^2P^o_{1/2}$			

A summary of positions, widths, and identifications of the major resonances obtained in the relativistic Breit-Pauli calculation on Ti^{3+} is given in Table VIII, along with a comparison with available experimental data [13,14]. In general, the agreement is quite good, especially for resonances in the lower energy region (below 45.50 eV) as regards both position and width. Note that some of the resonances listed in Table VIII can be reached by more than one initial state in the experimental mixture. They are listed more than once for purposes of comparison with the experimental results. That they are listed at different photons arises simply because each of the initial states has a different ionization energy so that differing photon energies are required from each of these initial states to excite a particular resonance (i.e., the difference in the resonance energies for a given resonance state in the table is just the difference in the binding energies of the initial states of the transitions).

Starting with V^{4+}, and continuing with other ions in the potassium isoelectronic sequence studied here, Cr^{5+}, Mn^{6+}, and Fe^{7+}, the Super-Coster-Kronig decay channel, that produces those giant ($3p \rightarrow 3d$) dipole resonances is closed because the $3p \rightarrow 3d$ excitation energy is below the ionization threshold; therefore, resonance structures observed in the photoionization cross-section spectra of those ions are much narrower than what we have seen in Sc^{2+} [36] and Ti^{3+} (previously mentioned). For each of those four ions, V^{4+}, Cr^{5+}, Mn^{6+}, and Fe^{7+}, the nonrelativistic calculations involve one initial state, the ground $[Ne]3s^2 3p^6 3d\ ^2D^e$ state, while in the relativistic (Breit-Pauli) calculations, we have two states, the ground state $[Ne]3s^2 3p^6 3d\ ^2D^e_{3/2}$ plus the first (metastable) excited state $[Ne]3s^2 3p^6 3d\ ^2D^e_{5/2}$.

Figure 7 shows the photoionization cross-section calculation results for V^{4+}. Figure 7(a) depicts the nonrelativistic calculations for the $[Ne]3s^2 3p^6 3d\ ^2D^e$ state, and the cross section is seen to be dominated by a series of Rydberg resonances associated with $3p$ excitation to a higher principal quantum number, since the $3p \rightarrow 3d\Delta n = 0$ transitions, unlike the Ti^{+3} case previously mentioned, lie below the ionization threshold; they are identified as $[(3p^5\ nd)\ 3d\ ^2P^o, ^2F^o]$ and $[(3p^5 n's)\ 3d\ ^2P^o, ^2F^o]$ (with $n \geqslant 4$ and $n' \geqslant 5$). The series limit is the excited V^{5+} $(3p^5 3d\ ^1P^o)$ state at photon energy 120.94 eV (120.44 eV from experiment [18]). Figure 7(b) gives the total cross sections from the ground $^2D^e_{3/2}$ state, and Fig. 7(c) shows the total cross sections from the excited $^2D^e_{5/2}$ state of V^{4+}. For both $^2D^e_{3/2}$ and $^2D^e_{5/2}$ states of V^{4+}, whose cross sections are shown in Figs. 7(b) and 7(c), respectively, the series of Rydberg resonances associated with $3p$ photoexcitation are $[(3p^5\ nd)\ 3d\ ^2P^o, ^2D^o, ^2F^o]$ and $[(3p^5 n's)\ 3d\ ^2P^o, ^2D^o, ^2F^o]$ (with $n \geqslant 4$ and $n' \geqslant 5$); note the difference between Figs. 7(b) and 7(c) on the one hand, and Fig. 7(a) on the other, is due to the transition $^2D^e \rightarrow\ ^2D^o$ which is forbidden in the nonrelativistic approach until photon energy 103.78 eV (103.43 eV in the experiment [18]). The fact that the difference is noticeable demonstrates the importance of relativistic interactions even at this (relatively) low Z.

Figures 8–10 show the present results for the photoionization cross sections for K-like ions Cr^{5+}, Mn^{6+}, and Fe^{7+}, respectively. The series of Rydberg resonances that dominate those spectra have their limit at the excited state Cr^{6+} $(3p^5 3d\ ^1P^o)$ at photon energy 152.39 eV (151.67 eV from experiment [18]) for Cr^{5+}, excited state Mn^{7+} $(3p^5 3d\ ^1P^o)$ at photon energy 186.87 eV (185.94 eV from experiment [18])

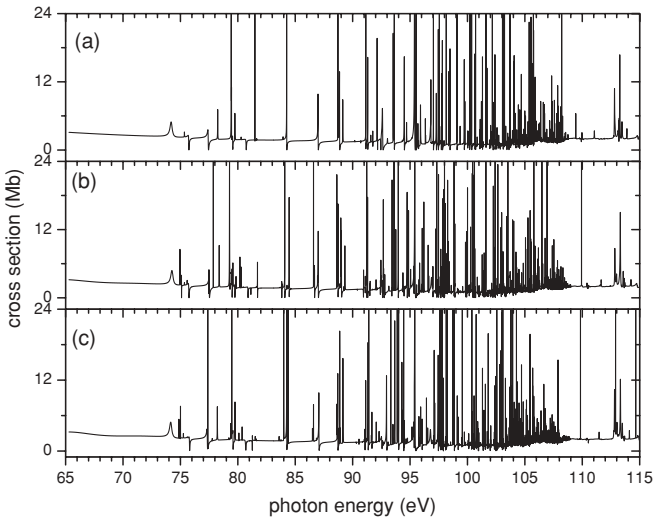

FIG. 7. Calculated V^{4+} photoionization cross sections showing (a) nonrelativistic (*LS*-coupling) cross sections from the initial ground state $^2D^e$, along with Breit-Pauli (relativistic) results for (b) the total ground $^2D^e_{3/2}$ state cross section, and (c) the total excited $^2D^e_{5/2}$ state cross section.

for Mn^{6+}, and excited state Fe^{8+} ($3p^5 3d\ ^1P^o$) at photon energy 224.39 eV (223.39 eV from experiment [18]) in the case of Fe^{7+}. In each case the nonrelativistic result for the $[Ne]3s^2 3p^6 3d\ ^2D^e$ state is shown in the upper panel, and the relativistic results for the ground $^2D^e_{3/2}$ state and the excited $^2D^e_{5/2}$ are shown in the lower panels. Clearly, the results for Cr^{5+}, Mn^{6+}, and Fe^{7+} are quite similar to the case of V^{4+} above.

To compare the various K-like transition metal ions, Sc^{2+} [36], Ti^{3+}, V^{4+}, Cr^{5+}, Mn^{6+}, and Fe^{7+}, the oscillator strength (Σ_f) sum [38,39] is investigated, in each case, in each of three different states ($^2D^e$, $^2D^e_{3/2}$, $^2D^e_{5/2}$) for photon energies between the lowest ionization threshold and the first $3p$ threshold. The results of our calculations are shown in Table IX.

Looking at results in Table IX, it is evident that the oscillator strength sum in the continuum decreases with increasing Z from $Z = 21$ to $Z = 26$; this occurs because, with increasing Z, more and more of the oscillator strength of the $3p \rightarrow 3d$ transitions move into the discrete (i.e., this strength goes into bound-bound transition, not photoionization). This movement into the discrete was clearly in evidence for Ti^{3+}, discussed above, where a $3p \rightarrow 3d$ resonance straddled the threshold with about 40% of it in the discrete region. For the next ion, V^{4+} ($Z = 23$) all of these resonant states that produce those giant ($3p \rightarrow 3d$ excitation) resonances become bound states and the oscillator strength in the continuum is seen to drop off sharply as compared to Sc^{2+} [36] and Ti^{3+} photoionization where almost all of the strength from the $3p^6$ subshell is owing to the giant $3p \rightarrow 3d$ resonances and lies in the continuum. For V^{4+}, Cr^{5+}, Mn^{6+}, and Fe^{7+} photoionization, although the giant $3p \rightarrow 3d$ resonances occur in the discrete (below threshold), for the outer-shell electron most of the oscillator strength remains predominantly in the continuum. This is

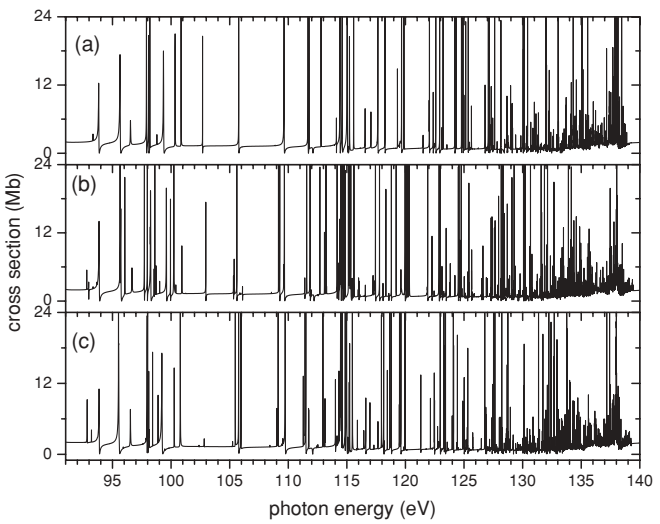

FIG. 8. The same as Fig. 7 but for Cr^{5+} photoionization cross sections.

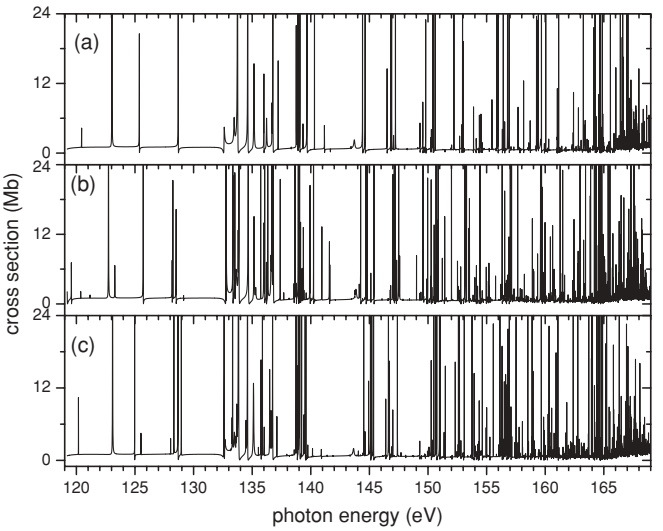

FIG. 9. The same as Fig. 7 but for Mn^{6+} photoionization cross sections.

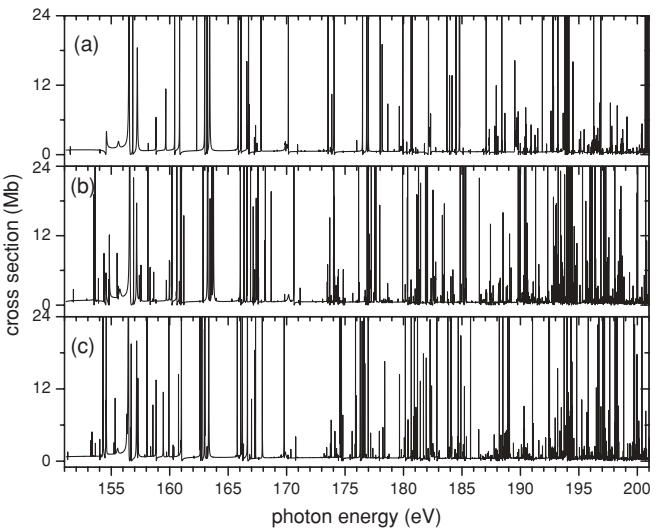

FIG. 10. The same as Fig. 7 but for Fe^{7+} photoionization cross sections.

TABLE IX. Oscillator strength sum for K-like transition metal ions Sc^{2+} [36], Ti^{3+}, V^{4+}, Cr^{5+}, Mn^{6+}, and Fe^{7+}, Σ_f, for $^2D^e$, $^2D^e_{3/2}$, $^2D^e_{5/2}$ states for photon energy from the lowest ionization threshold to the first $3p$ threshold.

K-like ions	Sc^{2+}	Ti^{3+}	V^{4+}	Cr^{5+}	Mn^{6+}	Fe^{7+}
Σ_f ($^2D^e$)	3.99	3.19	1.08	1.00	0.99	0.79
Σ_f($^2D^e_{3/2}$)	5.13	3.75	1.10	1.08	1.01	0.95
Σ_f ($^2D^e_{5/2}$)	5.44	4.26	1.12	1.09	1.03	0.94
Σ_f($^2D^e_{3/2}$) – Σ_f ($^2D^e$)	1.14	0.56	0.02	0.08	0.02	0.16
Σ_f ($^2D^e_{5/2}$) – Σ_f ($^2D^e$)	1.45	1.07	0.04	0.09	0.04	0.15

evident from Table IX where the oscillator strength sum for the four ions (V^{4+}, Cr^{5+}, Mn^{6+}, and Fe^{7+}) is close to 1 in each case. Note that the photoionization cross sections for V^{4+}, Cr^{5+}, Mn^{6+}, and Fe^{7+} are dominated by series of Rydberg resonances associated with $3p$ transitions to states with $n > 3$); since $\Delta n \neq 0$ for these transitions, the overlap (and dipole matrix element) between $3p$ orbital and nd orbital ($n > 3$) is small compared to the $\Delta n = 0$ case, so that these higher resonances are much weaker and narrower. Differences between the Sc^{2+} and Ti^{3+} cases, one hand, and V^{4+}, Cr^{5+}, Mn^{6+}, and Fe^{7+} on the other, in terms of continuum oscillator strength sum (Table IX) further confirms the importance of the contribution of these giant ($3p \rightarrow 3d$ excitation) resonances to the cross section of each of the K-like ions where they lie above the ionization threshold.

Furthermore, from Table IX, the two last lines [$\Sigma_f(^2D^e_{3/2}) - \Sigma_f$ ($^2D^e$) and Σ_f ($^2D^e_{5/2}$) – Σ_f ($^2D^e$)] show large differences between relativistic and nonrelativistic calculations for each of the K-like ions considered here; in each case, the relativistic oscillator strengths for Sc^{2+} and Ti^{3+} are quite large, of order unity, while for V^{4+}, Cr^{5+}, Mn^{6+}, and Fe^{7+} the differences are quite small. The large differences are due to the contributions of the $3p \rightarrow 3d$ dipole transition in the $^2D^e \rightarrow {}^2D^o$ channel which is forbidden in nonrelativistic (*LS*-coupling) theory below the first $3p$ ionization. This difference in continuum oscillator becomes far less important for the higher ions where all of the giant dipole oscillator strength is in the discrete. All of these observations are summarized in Fig. 11 which illustrates the evolution of the continuum oscillator strength sum with Z.

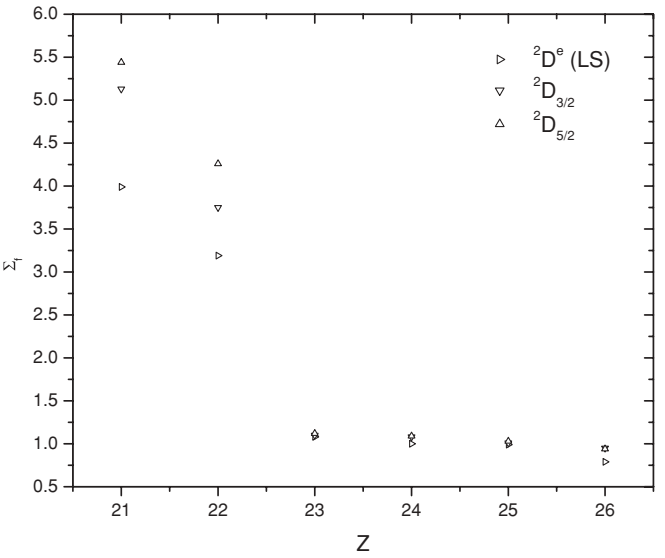

FIG. 11. Theoretical oscillator strength sum Σ_f as function of nuclear charge Z for $^2D^e$ (*LS*-coupling), $^2D^e_{3/2}$, and $^2D^e_{5/2}$ (Breit-Pauli) states for the photon energy range from the lowest ionization threshold to the first $3p$ threshold. Notice the dramatic decrease of Σ_f for $Z \geqslant 23$ compared to Σ_f for $Z = 21$ or 22. This is due to the important contribution to Σ_f from the giant dipole $3p \rightarrow 3d$ excitation dipole which lies in the continuum for $Z = 21$ and 22, but below threshold for $Z \geqslant 23$.

IV. CONCLUDING REMARKS

In this work, photoionization cross-section calculation results of the potassium-like transition metal ions Ti^{3+}, V^{4+}, Cr^{5+}, Mn^{6+}, and Fe^{7+} have been presented. For each of those ions, we have performed both nonrelativistic (*LS*-coupling) and relativistic (Breit-Pauli) calculations. While the photoionization cross-section spectra of Ti^{3+}, as for Sc^{2+} [36], are dominated by the giant ($3p \rightarrow 3d$ excitation) resonances, those of higher Z ($Z \geqslant 23$) ions (V^{4+}, Cr^{5+}, Mn^{6+}, and Fe^{7+}) are dominated by the Rydberg series of resonances since the $3p \rightarrow 3d$ resonances lie below the ionization threshold. This observation can be generalized, and extended to the last four members of the potassium isoelectronic sequence of the iron group (Co^{8+}, Ni^{9+}, Cu^{10+}, and Zn^{11+}); those four ions' photoionization cross-section spectra also are dominated by Rydberg series of resonances, and are the subject of a forthcoming work. Our theoretical results on Ti^{3+} showed good quantitative and qualitative agreement with available experimental data, and highlight the necessity to include core excitations ($3p$ excitation, in this case) in the description of transition processes in open d-subshell atoms or ions.

For Ti^{3+} the photoionization cross-section results on the excited [Ne]$3s^2 3p^6 4s\ ^2S^e_{1/2}$ state are presented, but there is no previous work to compare with; it would most interesting to have other results form (experimental or theoretical) to confirm our theoretical results. Furthermore, for the other four ions (V^{4+}, Cr^{5+}, Mn^{6+}, and Fe^{7+}) studied in this work, the same need for experimental data exists.

Aside from the specifics of the particular ions studied herein, the results can be broadly generalized to other systems as well. It is evident that, in general, along any isoelectronic sequence, more and more of the oscillator strength will move into the discrete region, with increasing Z. Since more of the oscillator strength is in the discrete excitation region, with increasing Z, there are fewer photoelectrons produced; this is important in the modeling of astrophysical and laboratory plasmas. In addition, it is also clear that the strength and width of resonances arising from $\Delta n = 0$ transitions are far far larger than the resonances which arise from transitions between states of different principal quantum number. This will be true for atoms and ions throughout the periodic table.

Another broad generalization can be made regarding the role of relativistic interactions at relatively low Z. These interactions were seen to cause splittings and shifts of thresholds and resonance positions, and these are not limited to the particular ions studied herein. In addition, it was found that,

in certain cases, the breakdown of *LS* coupling engendered by relativistic interactions opened photoionization channels that were absolutely forbidden within the context of *LS* coupling, and the cross sections of these *LS*-forbidden channels were not small. Clearly these phenomena, too, are quite general and not limited to the ions studied. Thus, for quantitative accuracy (and, in some situations, even qualitative accuracy) relativistic effects must be included in photoionization calculations of all atoms and ions with $Z \geqslant 20$ or so.

Finally, the experience of the present calculations has taught us that the representation of the wave function for the 3*d* electron is of crucial importance for these open 3*d*-subshell ions, owing to the fact that the effective *d*-wave potential has a double well [40]; this means that, depending upon the specific *LSJ* state, the 3*d* can be bound in the inner well, in the outer well, or balanced between them. Only for high enough *Z* that the 3*d* subshell is closed (or nearly closed) is the 3*d* bound in the inner well in all states and relatively insensitive in the specific *LSJ* state. This will be the case for all open-shell 3*d* atoms and ions, and for the 4*d* and 5*d* transition metals as well, and great care must be taken to expand these orbitals using a large enough basis set to be able to represent them accurately for all of the relevant *LSJ* states. And, the same will be true for open *f*-subshell atoms and ions; the *f*-wave potential is also double welled.

ACKNOWLEDGMENTS

We thank S. Schippers, A. Müller, R. A. Phaneuf, T. van Zoest, I. Álvarez, C. Cisneros, E. D. Emmons, M. F. Gharaibeh, G. Hinojosa, A. S. Schlachter, and S. W. J. Scully for supplying their Ti^{3+} photoionization data in numerical form and for numerous discussions. We also express our gratitude to T. W. Gorczyca for discussion and suggestions about our Ti^{3+} calculation results, along with Dragan Nikolić for providing numerical data. In addition, we thank N. Badnell for making available on his very comprehensive Web site all the codes on *R*-matrix used in this work. We finally thank A. Hibbert for assistance and discussions concerning all those target orbitals used in the K-like ions PI calculations. The calculations were performed using the computational facilities at the National Energy Research Scientific Computing Center (NERSC). This work was supported by the Department of Energy, division of Chemical Sciences, and the National Science Foundation.

[1] B. Sonntag and P. Zimmerman, Rep. Prog. Phys. **55**, 911 (1992).
[2] *New Directions in Research with Third-Generation Soft X-Ray Synchrotron Radiation Sources*, Vol. 254, NATO Advanced Study Institute Series E: Applied Sciences, edited by A. S. Schlachter and F. J. Wuilleumier (Kluwer, Dordtecht, 1992).
[3] M. Martins, K. Godenusen, T. Richter, P. Wemet, and P. Zimmermann, J. Phys. B: At. Mol. Phys. **39**, R79 (2006).
[4] H. Kjeldsen, J. Phys. B: At. Mol. Phys. **39**, R325 (2006).
[5] W. Eissner, M. Jones, and H. Nussbaumer, Comput. Phys. Commun. **8**, 270 (1974).
[6] N. R. Badnell, J. Phys. B **19**, 3827 (1986).
[7] N. R. Badnell, J. Phys. B **30**, 1 (1997).
[8] UK APAP Codes [http://amdpp.phys.strath.ac.uk/tamoc/code.html].
[9] P. G. Burke, C. J. Noble, and V. M. Burke, Adv. At. Mol. Opt. Phys. **54**, 237 (2006).
[10] K. Berrington, L. Quigley, and J. Pelan, Comput. Phys. Commun. **114**, 225 (1998).
[11] L. Quigley and K. Berrington, J. Phys. B **29**, 4529 (1996).
[12] J. M. Ramirez and M. A. Bautista, J. Phys. B **35**, 4139 (2002).
[13] S. Schippers *et al.*, J. Phys. B **37**, L209 (2004).
[14] A. N. Ryabtsev, S. S. Churilov, and Ya É. Kononov, Opt. Spectrosc. **98**, 519 (2005).
[15] K. A. Berrington, W. B. Eissner, and P. H. Norrington, Comput. Phys. Commun. **92**, 290 (1995).
[16] K. A. Berrington, P. G. Burke, J. J. Chang, A. T. Chivers, W. D. Robb, and K. T. Taylor, Comput. Phys. Commun. **8**, 149 (1974).
[17] K. A. Berrington, P. G. Burke, M. LeDourneuf, W. D. Robb, K. T. Taylor, and Vo Ky Lan, Comput. Phys. Commun. **14**, 367 (1978).
[18] NIST [http://physics.nist.gov/PhysRefData/ASD/levels_form.html].
[19] D. Nikolić, T. W. Gorczyca, and N. R. Badnell, Phys. Rev. A **79**, 012703 (2009).
[20] P. G. Burke and K. A. Berrington, *Atomic and Molecular Processes: An R-matrix Approach* (IOP Publishing, Bristol, 1993).
[21] P. G. Burke and W. D. Robb, Adv. At. Mol. Phys. **11**, 143 (1976).
[22] G. Breit and E. P. Wigner, Phys. Rev. **49**, 519 (1936).
[23] S. N. Tiwary, A. E. Kingston, and A. Hibbert, J. Phys. B: At. Mol. Phys. **16**, 2457 (1983).
[24] T. W. Gorczyca, M. S. Pindzola, D. C. Griffin, and N. R. Badnell, J. Phys. B: At. Mol. Phys. **27**, 2399 (1994).
[25] W. Eissner, N. Huu Hoa, and L. Vo Ky, *Calculations of Photoionization on Ti^{3+}* (ICPEAC Abstract, Kalamazoo, 2009).
[26] R. F. Reilman and S. T. Manson, Astrophys. J. Suppl. Ser. **40**, 815 (1979).
[27] S. Schippers *et al.*, Phys. Rev. Lett. **89**, 193002 (2002).
[28] S. Schippers *et al.*, Phys. Rev. A **67**, 032702 (2003).
[29] I. C. Lyon, B. Peart, K. Dolder, and J. B. West, J. Phys. B: At. Mol. Phys. **20**, 1471 (1987).
[30] A. Müller, S. Schippers, A. M. Covington, A. Aguilar, G. Hinojosa, R. A. Phaneuf, M. M. SantAnna, A. S. Schlachter, J. D. Bozek, and C. Cisneros, *2001 XXII International Conference on Photonic, Electronic and Atomic Collisions*, *Santa Fe, New Mexico, 18–24 July, 2001*, *Abstracts of Contributed Papers*, edited by S. Datz, M. E. Bannister, H. F. Krause, L. H. Saddiq, D. Schultz, and C. R. Vane (Rinton, Princeton, 2001), p. 52.
[31] H. Kjeldsen, F. Folkmann, F. Innocenti, L. Zuin, and J. E. Hansen, J. Phys. B: At. Mol. Phys. **35**, L375 (2002).
[32] J. B. West, H. Kjeldsen, F. Folkmann, and T. Andersen, J. Phys. B: At. Mol. Phys. **34**, 4035 (2001).

[33] J. E. Hansen, H. Kjeldsen, F. Folkmann, M. Martins, and J. B. West, J. Phys. B: At. Mol. Phys. **40**, 293 (2007).
[34] A. Hibbert and J. E. Hansien, J. Phys. B: At. Mol. Opt. Phys. **32**, 4133 (1999).
[35] A. M. Sossah, H.-L. Zhou, and S. T. Manson (in preparation).
[36] A. M. Sossah, H.-L. Zhou, and S. T. Manson, Phys. Rev. A **78**, 053405 (2008).
[37] J. Zeng, G. Zhao, and J. Yuan, Phys. Rev. A **68**, 022714 (2003).
[38] H. A. Bethe and E. E. Salpeter, *Quantum Mechanics of One- and Two-Electron Atoms* (Springer-Verlag, Berlin, 1957).
[39] J. Berkowitz, *Photoabsorption, Photoionization, and Photoelectron Spectroscopy* (Academic Press, New York, 1979).
[40] A. R. P. Rau and U. Fano, Phys. Rev. **167**, 7 (1968).